

Aberrations of flat lenses and aplanatic metasurfaces

Francesco Aieta,¹ Patrice Genevet,¹ Mikhail Kats¹ and Federico Capasso^{1,*}

¹*School of Engineering and Applied Sciences, Harvard University, Cambridge, Massachusetts 02138, USA*

**capasso@seas.harvard.edu*

Abstract: A study of optical aberrations for flat lenses based on phase discontinuities is reported. The wave aberration function and the analytical expression of the aberrations up to the 4th order are derived to describe the performance of both ideal and practical flat lenses. We find that aberration-free focusing is possible under axial illumination but off-axis aberrations appear when the excitation is not normal to the interface. An alternative design for an aplanatic metasurface on a curved substrate is proposed to focus light without coma and spherical aberrations.

©2013 Optical Society of America

OCIS codes: (080.1010) Aberrations (global); (250.5403) Plasmonics; (080.3630) Lenses; (160.3918) Metamaterials.

References and Links

1. C. L. Holloway, A. Dienstfrey, E. F. Kuester, J. F. O'Hara, A. K. Azad, and A. J. Taylor, "A discussion on the interpretation and characterization of metafilms/metamaterials: The two-dimensional equivalent of metamaterials," *Metamaterials (Amst.)* **3**(2), 100–112 (2009).
2. N. Yu, P. Genevet, M. A. Kats, F. Aieta, J.-P. Tetienne, F. Capasso, and Z. Gaburro, "Light propagation with phase discontinuities: generalized laws of reflection and refraction," *Science* **334**(6054), 333–337 (2011).
3. N. Yu, P. Genevet, F. Aieta, M. A. Kats, R. Blanchard, G. Aoust, J.-P. Tetienne, Z. Gaburro, and F. Capasso, "Flat optics: controlling wavefronts with optical antenna metasurfaces," *IEEE J. Sel. Top. Quantum Electron.* **19**(3), 4700423 (2013).
4. A. V. Zayats and S. Maier, *Active Plasmonics and Tuneable Plasmonic Metamaterials* (Wiley, 2013)
5. A. V. Kildishev, A. Boltasseva, and V. M. Shalaev, "Planar photonics with metasurfaces," *Science* **339**(6125), 1232009 (2013).
6. S. Q. Sun, Q. He, S. Xiao, Q. Xu, X. Li, and L. Zhou, "Gradient-index meta-surfaces as a bridge linking propagating waves and surface waves," *Nat. Mater.* **11**(5), 426–431 (2012).
7. C. Pfeiffer and A. Grbic, "Metamaterial Huygens' surfaces: tailoring wave fronts with reflectionless sheets," *Phys. Rev. Lett.* **110**(19), 197401 (2013).
8. A. Papakostas, A. Potts, D. M. Bagnall, S. L. Prosvirnin, H. J. Coles, and N. I. Zheludev, "Optical manifestations of planar chirality," *Phys. Rev. Lett.* **90**(10), 107404 (2003).
9. M. Kats, P. Genevet, G. Aoust, N. Yu, R. Blanchard, F. Aieta, Z. Gaburro, and F. Capasso, "Giant birefringence in optical antenna arrays with widely tailorable optical anisotropy," *Proc. Natl. Acad. Sci. U.S.A.* **109**(31), 12364–12368 (2012).
10. N. Engheta and R. W. Ziolkowski, *Metamaterials: Physics and Engineering Explorations* (Wiley-Interscience, 2006).
11. M. Agio and A. Alù, *Optical Antennas* (Cambridge, 2013)
12. F. Aieta, P. Genevet, M. A. Kats, N. Yu, R. Blanchard, Z. Gaburro, and F. Capasso, "Aberration-free ultrathin flat lenses and axicons at telecom wavelengths based on plasmonic metasurfaces," *Nano Lett.* **12**(9), 4932–4936 (2012).
13. B. Memarzadeh and H. Mosallaei, "Array of planar plasmonic scatterers functioning as light concentrator," *Opt. Lett.* **36**(13), 2569–2571 (2011).
14. X. Chen, L. Huang, H. Mühlenbernd, G. Li, B. Bai, Q. Tan, G. Jin, C.-W. Qiu, S. Zhang, and T. Zentgraf, "Dual-polarity plasmonic metalens for visible light," *Nat. Commun.* **3**, 1198 (2012).
15. M. Kang, T. Feng, H.-T. Wang, and J. Li, "Wave front engineering from an array of thin aperture antennas," *Opt. Express* **20**(14), 15882–15890 (2012).
16. A. Pors, M. G. Nielsen, R. L. Eriksen, and S. I. Bozhevolnyi, "Broadband focusing flat mirrors based on plasmonic gradient metasurfaces," *Nano Lett.* **13**(2), 829–834 (2013).
17. X. Li, S. Xiao, B. Cai, Q. He, T. J. Cui, and L. Zhou, "Flat metasurfaces to focus electromagnetic waves in reflection geometry," *Opt. Lett.* **37**(23), 4940–4942 (2012).
18. X. Ni, S. Ishii, A. V. Kildishev, and V. M. Shalaev, "Ultra-thin, planar, Babinet-inverted plasmonic metalenses," *Light Sci. Appl.* **2**(4), e72 (2013).

19. C. Pfeiffer and A. Grbic, "Cascaded metasurfaces for complete phase and polarization control," *Appl. Phys. Lett.* **102**(23), 231116 (2013).
20. F. Aieta, P. Genevet, N. Yu, M. A. Kats, Z. Gaburro, and F. Capasso, "Out-of-plane reflection and refraction of light by anisotropic optical antenna metasurfaces with phase discontinuities," *Nano Lett.* **12**(3), 1702–1706 (2012).
21. S. K.-Y. Sun, K. Y. Yang, C. M. Wang, T. K. Juan, W. T. Chen, C. Y. Liao, Q. He, S. Xiao, W. T. Kung, G. Y. Guo, L. Zhou, and D. P. Tsai, "High-efficiency broadband anomalous reflection by gradient meta-surfaces," *Nano Lett.* **12**(12), 6223–6229 (2012).
22. X. Ni, N. K. Emani, A. V. Kildishev, A. Boltasseva, and V. M. Shalaev, "Broadband light bending with plasmonic nanoantennas," *Science* **335**(6067), 427 (2012).
23. S. Larouche and D. R. Smith, "Reconciliation of generalized refraction with diffraction theory," *Opt. Lett.* **37**(12), 2391–2393 (2012).
24. Z. Wei, Y. Cao, X. Su, Z. Gong, Y. Long, and H. Li, "Highly efficient beam steering with a transparent metasurface," *Opt. Express* **21**(9), 10739–10745 (2013).
25. P. Genevet, N. Yu, F. Aieta, J. Lin, M. A. Kats, R. Blanchard, M. O. Scully, Z. Gaburro, and F. Capasso, "Ultra-thin plasmonic optical vortex plate based on phase discontinuities," *Appl. Phys. Lett.* **100**(1), 013101 (2012).
26. J. He, X. Wang, D. Hu, J. Ye, S. Feng, Q. Kan, and Y. Zhang, "Generation and evolution of the terahertz vortex beam," *Opt. Express* **21**(17), 20230–20239 (2013).
27. N. Yu, F. Aieta, P. Genevet, M. A. Kats, Z. Gaburro, and F. Capasso, "A broadband, background-free quarter-wave plate based on plasmonic metasurfaces," *Nano Lett.* **12**(12), 6328–6333 (2012).
28. Y. Zhao, M. A. Belkin, and A. Alù, "Twisted optical metamaterials for planarized ultrathin broadband circular polarizers," *Nat. Commun.* **3**, 870 (2012).
29. B. Yang, W. M. Ye, X. D. Yuan, Z. H. Zhu, and C. Zeng, "Design of ultrathin plasmonic quarter-wave plate based on period coupling," *Opt. Lett.* **38**(5), 679–681 (2013).
30. F. Zhou, Y. Liu, and W. Cai, "Plasmonic holographic imaging with V-shaped nanoantenna array," *Opt. Express* **21**(4), 4348–4354 (2013).
31. H. Gross, *Handbook of Optical Systems: Aberration Theory and Correction of Optical Systems* (Wiley-VCH, 2007).
32. M. Young, "Zone plates and their aberrations," *J. Opt. Soc. Am. A* **62**(8), 972 (1972).
33. A. Maréchal, "Mechanical integrator for studying the distribution of light in the optical image," *J. Opt. Soc. Am.* **37**, 403 (1947).
34. M. Born and E. Wolf, *Principles of Optics: Electromagnetic Theory of Propagation, Interference and Diffraction of Light*, 2nd ed. (New York Pergamon, 1999).
35. M. V. R. K. Murty, "Spherical zone-plate diffraction grating," *J. Opt. Soc. Am.* **50**(9), 923 (1960).
36. P. Artal, J. Santamaría, and J. Bescós, "Retrieval of wave aberration of human eyes from actual point-spread-function data," *J. Opt. Soc. Am. A* **5**(8), 1201–1206 (1988).
37. M. Lombardo and G. Lombardo, "Wave aberration of human eyes and new descriptors of image optical quality and visual performance," *J. Cataract Refract. Surg.* **36**(2), 313–331 (2010).
38. C. Roddier and F. Roddier, "Wave-front reconstruction from defocused images and the testing of ground-based optical telescopes," *J. Opt. Soc. Am. A* **10**(11), 2277–2287 (1993).
39. W. Coene, G. Janssen, M. O. de Beek, D. Van Dyck, "Phase retrieval through focus variation for ultra-resolution in field-emission electron microscopy," *Phys. Rev. Lett.* **69**(26), 3743–3746 (1992).
40. F. Hosokawa, T. Tomita, M. Naruse, T. Honda, P. Hartel, and M. Haider, "A spherical aberration-corrected 200 kV TEM," *J. Electron Microsc. (Tokyo)* **52**(1), 3–10 (2003).
41. R. Fischer, *Optical System Design*, 2nd ed. (McGraw-Hill Professional, 2008).
42. J. W. Goodman, *Introduction to Fourier Optics*, 3rd ed. (Roberts & Company, 2005).
43. E. Hecht, *Optics*, 4th (Wesley Publishing Company 2001).
44. J. Tetienne, R. Blanchard, N. Yu, P. Genevet, M. A. Kats, J. A. Fan, T. Edamura, S. Furuta, M. Yamanishi, and F. Capasso, "Dipolar modeling and experimental demonstration of multi-beam plasmonic collimators," *New J. Phys.* **13**(5), 053057 (2011).
45. J. J. W. Bruce and P. J. Giblin, *Curves and Singularities: A Geometrical Introduction to Singularity Theory* (Cambridge University, 1992).
46. B. Kress and P. Meyrueis, *Applied Digital Optics* (Wiley, 2009).
47. D. B. Murphy and M. W. Davidson, *Fundamentals of Light Microscopy and Electronic Imaging* (John Wiley & Sons, 2012).
48. R. Kingslake and R. B. Johnson, *Lens Design Fundamentals*, 2nd ed. (Academic, 2009).
49. L. S. Shively, *An Introduction to Modern Geometry* (John Wiley & Sons, Inc., 1953).
50. F. Aieta, A. Kabiri, P. Genevet, N. Yu, M. A. Kats, Z. Gaburro, and F. Capasso, "Reflection and refraction of light from metasurfaces with phase discontinuities," *J. Nanophotonics* **6**, 063532 (2012).
51. P. Ruchhoeft, M. Colburn, B. Choi, H. Nounu, S. Johnson, T. Bailey, S. Damle, M. Stewart, J. Ekerdt, S. V. Sreenivasan, J. C. Wolfe, and C. G. Willson, "Patterning curved surfaces: template generation by ion beam proximity lithography and relief transfer by step and flash imprint lithography," *J. Vac. Sci. Technol. B* **17**, 2965–2969 (1999).
52. B. D. Gates, Q. Xu, M. Stewart, D. Ryan, C. G. Willson, and G. M. Whitesides, "New approaches to nanofabrication: molding, printing, and other techniques," *Chem. Rev.* **105**(4), 1171–1196 (2005).

53. D. Radtke and U. D. Zeitner, "Laser-lithography on non-planar surfaces," *Opt. Express* **15**(3), 1167–1174 (2007).
 54. B. Päivänranta, M. Pudas, O. Pitkänen, K. Leinonen, M. Kuittinen, P.-Y. Baroni, T. Scharf, and H.-P. Herzig, "Liquid phase deposition of polymers on arbitrary shaped surfaces and their suitability for e-beam patterning," *Nanotechnology* **20**(22), 225305 (2009).
 55. E. J. Smythe, M. D. Dickey, G. M. Whitesides, and F. Capasso, "A Technique to transfer metallic nanoscale patterns to small and non-planar surfaces," *ACS Nano* **3**(1), 59–65 (2009).
 56. E. J. Smythe, M. D. Dickey, J. Bao, G. M. Whitesides, and F. Capasso, "Optical antenna arrays on a fiber facet for in situ surface-enhanced Raman scattering detection," *Nano Lett.* **9**(3), 1132–1138 (2009).
 57. K. E. Paul, M. Prentiss, and G. M. Whitesides, "Patterning spherical surfaces at the two-hundred-nanometer scale using soft lithography," *Adv. Funct. Mater.* **13**(4), 259–263 (2003).
-

1. Introduction

Optical metasurfaces are artificial interfaces designed to manipulate light at the subwavelength scale and exhibit functionalities not attainable with conventional optical components [1–9]. While metamaterials are typically three-dimensional structures [10], metasurfaces are characterized by a two-dimensional layout that is compatible with most of the planar manufacturing techniques and may enable new flat optical devices [3,5]. In the case of metasurfaces composed of inhomogeneous arrays of optical resonators with subwavelength separation [2,9,11] the wavefront of scattered light can be reshaped and redirected at will depending on the array design. Each resonator introduces locally an abrupt phase shift over the scale of the wavelength of the scattered wavefront, dubbed phase discontinuities. Such metasurfaces can reproduce many functionalities that are usually attained by combining refractive optical components. To date devices such as flat lenses [12–19], axicons [12], blazed gratings [2,20–24], vortex plates [24,25], plates for polarization control [27–29] and holographic plates [30] have been demonstrated. Different types of resonators can be implemented to create a metasurface: V-shaped antennas [2,3,12], nano-apertures [15,24,26], patch antennas [13,16,17], dipole antennas [14], dielectric resonators [1], etc.

We have recently shown that a hyperboloidal distribution of phase discontinuities at an interface creates a spherical wavefront to focus light at the desired focal distance [12]. The subwavelength control over the phase front provided by the metasurface allows for the design of flat lenses with high numerical aperture (NA) that focus light under axial (i.e. normal) illumination without aberrations. However, for illumination non-parallel to the optical axis, diffraction-limited focusing is not possible due to off-axis aberrations. In the practical realization of a flat lens [12], the metasurface is approximated by a discrete rather than continuous distribution of phase discontinuities; this implies small deviations from the spherical wavefront.

This article contains a quantitative analysis of the primary monochromatic aberrations associated with flat lenses based on metasurfaces. We prove that for a continuous phase profile and normal incidence the lens is aberration-free, while for off-axis illumination coma and other aberrations appear, though it remains free from spherical aberrations and distortion [31,32]. The effect of the discretization of the phase profile is evaluated and it is shown that four elements are enough to guarantee an imaging quality limited only by diffraction of light [33,34]. Following the approach proposed in [35] by Murty for Fresnel zone plates, we present a design for a curved metasurface-based lens that can focus light without spherical aberrations and coma, defined as aplanatic metasurface. Chromatic aberrations are not considered here and will be treated separately in future work.

2. Aberrations of flat lenses

Optical aberrations arise in optical systems whenever the rays emerging from a point object do not meet all at the same image point. There exist many ways to describe aberrations [31,34]; the wave aberration function (WAF) is one of the most commonly used to study aberrations in human eyes [36,37], telescopes [38] and electron microscopes [39,40]. The main advantage of the WAF is that it can be directly accessed via interferometric

measurements. Rather than tracing the rays that form an image, WAF represent the difference between the wavefront and an ideal, aberration-free wavefront, i.e. a reference sphere centered in the object point [31,41]. While for an ideal lens $WAF = 0$, in most applications a limited amount of aberrations can be tolerated in light of the fact that the resolution of any optical system has an upper limit given by diffraction. The Maréchal criterion [31,33,34], stipulates that when $WAF_{rms} = \langle WAF \rangle^2 - \langle WAF^2 \rangle$ is less than $\lambda/14$, where the brackets represent the mean value and λ is the wavelength, the dominant factor limiting the imaging quality is diffraction and therefore, for most applications, aberrations are negligible [34]. The presence of aberrations can be easily visualized using the point spread function (PSF), defined as the image of a point object [42]. If the focusing wavefront differs from the reference sphere, the PSF will deviate from the ideal Airy disk; the Strehl ratio, defined as the ratio between the peak of the PSF and the peak of the PSF of an aberrations-free lens, is used to quantify this deviation. The modulation transfer function (MTF) provides a characterization of an optical system in the spatial frequency domain; it is defined as the modulus of the Fourier transform of the PSF and it shows the normalized contrast transferred by the lens from the object to its image [43]. If we consider an object made of periodic black and white line pairs, the MTF indicates how blurred they will be imaged by the lens, as a function of their periodicity. In the following these definitions are used to characterize metasurface-based lenses.

When a light beam is incident on a metasurface, it is scattered by each element individually, and the sum of all of these components will determine the overall transmitted wavefront. We can approximate locally the wavefront scattered by each subwavelength metasurface-element as a spherical wavelet whose radius R is proportional to the phase shift φ of the scattered field with respect to the incident wave [Fig. 1(a)] [12,44]. In the case of a hyperboloidal distribution of phase discontinuities of a flat lens as given in Eq. (1) of [12], the radius of each spherical wave at every position of the metasurface (t_x, t_y) is given by:

$$R(t_x, t_y) = \frac{\lambda}{2\pi} \varphi(t_x, t_y) = \sqrt{t_x^2 + t_y^2 + f^2} - f \quad (1)$$

where f is the focal length. Based on the Huygens' principle, the resulting wavefront can be obtained from the envelope of the secondary wavelets [7,42]. Let us consider a plane wave propagating parallel to the optical axis and incident on the metasurface; the family of curves describing the spherical waves leaving every element of the metasurface is:

$$F(x, y, z, t_x, t_y) = (x - t_x)^2 + (y - t_y)^2 + z^2 - R(t_x, t_y)^2 \quad (2)$$

with $x^2 + y^2 \leq \rho$, ρ is the radius of the flat lens. The envelope of Eq. (2) is calculated by imposing F and the partial derivatives $\partial_x F$ and $\partial_y F$ equal to zero [45] which gives:

$$x^2 + y^2 + (z - f)^2 = f^2 \quad (3)$$

Equation (3) describes the surface of the spherical-aberration-free wavefront generated by the flat lens. Therefore we conclude that the WAF is zero and the flat lens can focus without aberrations when used to image a distant point on the optical axis.

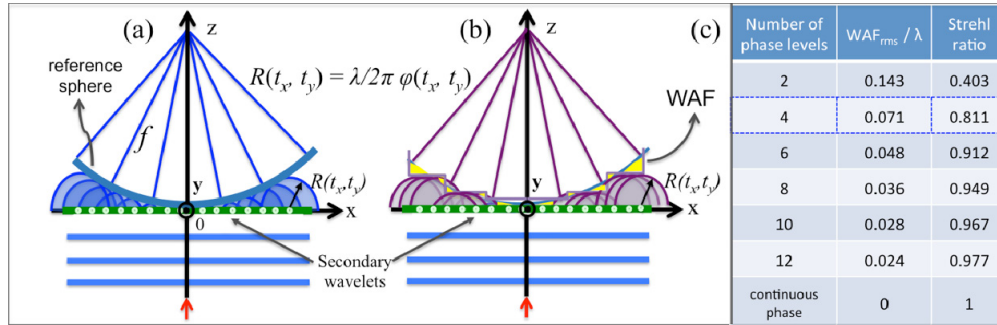


Fig. 1. (a) The wavefront scattered by a flat lens based on a metasurface is given by the envelope of the secondary spherical waves emitted by the antennas with subwavelength separation. For a very dense distribution of antennas, the phase function $\varphi(x, y)$ can be assumed continuous leading to a perfect spherical wavefront. (b) If a flat lens is designed using a limited set of phase elements, the continuous phase function is replaced with a discrete distribution that introduces aberrations (the yellow region corresponds to the wave aberration function (WAF)). (c) The effect of the discretization of the phase function is evaluated by calculating the root mean square of the wave aberration function (WAF_{rms}) and the Strehl ratio for an increasing number of phase levels.

In a real implementation of a flat lens it is convenient to use a limited set of elements that cover the phase range 0-to- 2π by replacing the target phase distribution with an approximated step-function whose accuracy depends on the number of elements (i.e. phase levels) used. For example, in [12], the hyperboloidal distribution was approximated using a set of 8 elements with incremental phase of $\pi/4$. This approximation introduces slight variations to the wavefront compared to an ideal converging wave [Fig. 1(b)]. In order to quantify the effect of this finite phase resolution, we calculate the WAF_{rms} for a flat lens with a hyperboloidal phase distribution for an increasing number of phase levels [Fig. 1(c)]. The results show that four levels of phase ($0, \pi/2, \pi, 3\pi/2$) are sufficient to satisfy the Maréchal criterion. For an increasing number of phase levels the WAF rapidly approaches the aberration-free limit of continuous phase. We also calculate the Strehl ratio that shows that for a flat lens with more than 4 discrete elements, the deviation from the Airy disk becomes negligible (Strehl ratio > 0.8) [Fig. 1(c)] [34]. Similar considerations regarding the trade-off between the approximation of the phase distribution and diffraction efficiency are known in the context of diffractive Fresnel lenses (i.e. Fresnel lenses with a finite number of thickness levels instead of a continuous profile), where a higher number of phase levels can be obtained at the cost of increasing the number of consecutive fabrication steps [46]. Based on the application requirements, a flat metasurface-based lens can be made with a large number of phase levels in a single fabrication step, i.e. using a single mask.

3. Off-axis aberrations

In the following we will analyze the primary aberrations of a flat lens with continuous phase distribution in the case of oblique illumination, which are particularly relevant for applications requiring a wide field of view [Fig. 2(a)]. We start with the analytical derivation of primary aberrations from the difference in optical path (OPD) between a marginal ray and the axial ray passing through the center of the flat lens (*chief ray*). For simplicity we restrict the derivation to two dimensions only ($r = \sqrt{x^2 + y^2}, z$) following the procedure used by Young in [32]. The rays refract when entering the substrate and then, once they reach the metasurface, they are directed towards the focus due to the effect of the phase distribution. The angle formed by each ray can be found by applying the generalized law of refraction with the local value of phase gradient [2,20]. The OPD between the marginal and the chief ray is calculated by

subtracting the optical path corresponding to the yellow segment, from the sum of the optical paths corresponding to the red segments and the equivalent optical path associated with the phase discontinuity at the point r : $\frac{\lambda}{2\pi}\varphi(r)$ [Fig. 2(a)]. We expand the expression obtained in a polynomial series obtaining [32]:

$$OPD = -\frac{1}{4f}r^2\alpha^2 - \frac{5}{4f}r^2\alpha^2 - \frac{1}{4f^2}r^3\alpha + \text{higher order terms} \quad (4)$$

where α is the illumination angle and r is the transverse coordinate. Only the terms corresponding to the Seidel aberrations are retained. The first term on the right hand side of Eq. (4) is the *Petzval field curvature*, the second is *astigmatism*, while the third is *coma*. The latter is often regarded as the most problematic in microscopy due to the asymmetry produced in the image. Note that no spherical aberrations or image distortions are present [31,32].

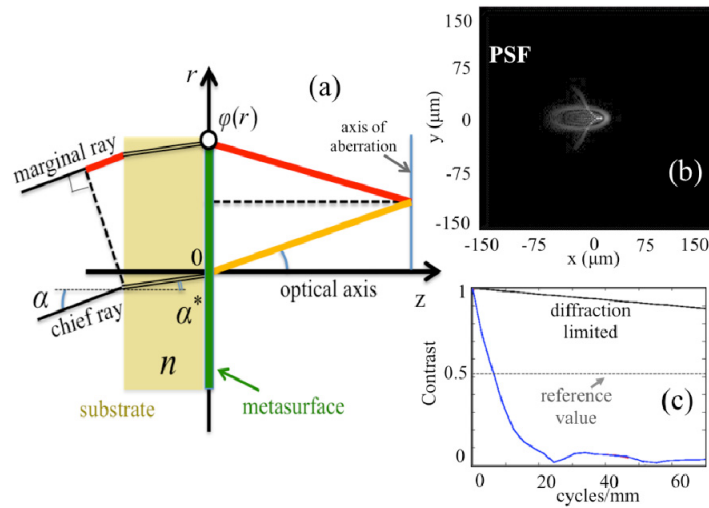


Fig. 2. (a) A flat lens is illuminated with parallel light incident at angle α with the optical axis. An axial ray (chief ray) and a marginal ray are refracted at an angle α^* in the substrate (with refractive index n). $\varphi(r)$ is the phase shift at point r , with respect to the center of the lens ($r = 0$). (b) Point Spread Function (PSF) calculated from the WAF for a flat lens with radius 1 mm, $NA = 0.5$ illuminated with parallel monochromatic light at $\lambda = 1.55 \mu\text{m}$ incident at an angle $\alpha = 10^\circ$. x and y are the spatial coordinates in the focal plane. (c) Modulation Transfer Function (MTF) (blue curve) for the same lens. The MTF for an aberration-free lens with the same NA is shown for comparison.

To validate the results of the analytical derivation, we perform a numerical study of a flat lens under oblique illumination. We calculate the WAF, PSF and MTF for a circular flat lens with radius $\rho = 1 \text{ mm}$, $NA = 0.5$ illuminated with parallel monochromatic light at $\lambda = 1.55 \mu\text{m}$ incident at an angle $\alpha = 10^\circ$. Figure 2(b) shows how the PSF deviates from the ideal Airy disc, forming an asymmetrical comet-like spot, as expected for a comatic optical system [43]. In [Fig. 2(c)] we show the projection of the MTF along the axis of aberration (the axis, in the image plane, that intersects the chief ray and the optical axis). In order to interpret this result we should consider that the minimum contrast needed by a detector to resolve spatial frequencies varies with other factors such as brightness of the image [37]. If we fix a reference value for the minimum contrast at 0.5, the resolution of the flat lens under this condition of illumination can reach 8 cycles/mm (number of line pairs per millimeter). Note that the upper limit for a lens with the same NA would be a resolution of 320 cycles/mm by

maintaining a contrast of 0.5, as can be obtained by extrapolating the MTF for a diffraction limited lens [Fig. 2(c)].

4. Aplanatic metasurface

An aplanatic lens, is a lens corrected for both spherical aberrations and coma; this type of lens is widely used in microscope objectives and condenser lenses [43,47]. Following the approach developed by Murty [35] for Fresnel zone plates, we propose a design for an aplanatic lens based on a metasurface.

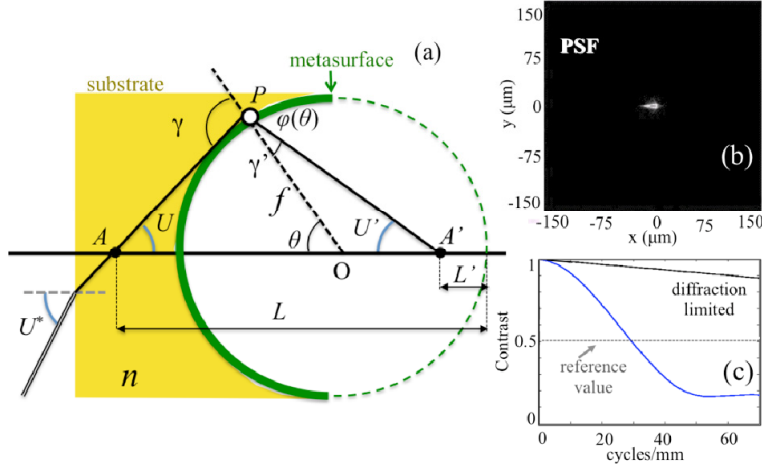


Fig. 3. (a) Schematic of the aplanatic metasurface patterned on a spherical interface with center in O and with radius f . According to the definition of Apollonius, the locus of points that have a specified ratio of the distances between two fixed points (A and A') known as foci, is a circle. A ray incident on the substrate at an angle U^* is refracted and hits the metasurface in point P. We derived the expression of the phase gradient which imposes at the point P the proper phase such that a ray forming an angle U with the optical axis is redirected to form an angle U' with the optical axis. (b) Point Spread Function (PSF) and (c) Modulation Transfer Function (MTF) for an aplanatic metasurface with $NA = 0.5$ illuminated with parallel monochromatic light at $\lambda = 1.55 \mu\text{m}$ incident at an angle $\alpha = 10^\circ$.

The Abbe sine condition establishes that an optical system corrected for spherical aberrations will also be free from coma if the ratio between the sine of the angle traced by a ray as it leaves the object and the sine of the angle traced by the same ray as it reaches the image plane is constant for all the rays [48]. With reference to Fig. 3(a), given an object ray \overline{AP} and the corresponding image ray $\overline{A'P}$, it follows from the definition of circle given by Apollonius [49] that if the point of intersection P lies on the surface of a circle, the ratio $\overline{AP} / \overline{A'P} = \sin U' / \sin U = L / L' = M$ is constant, automatically satisfying the Abbe Sine condition. Therefore it is possible to design an aplanatic lens by patterning the metasurface on a spherical interface. From the generalized law of refraction for spherical interfaces [50], we can calculate the phase gradient required for an object ray forming an angle U with the optical axis to produce an image ray forming the angle U' .

The generalized law of refraction applied at point P [Fig. 3(a)] reads:

$$-n \sin \gamma + \sin \gamma' = \frac{\lambda}{2\pi} \frac{d\phi}{d\theta} \quad (5)$$

As shown by Murty in [35], from geometrical identities we can write:

$$\begin{cases} \sin \gamma = \frac{L-f}{AP} \sin \theta \\ \sin \gamma' = \frac{f-L'}{A'P} \sin \theta \end{cases} \quad (6)$$

Given the presence of the substrate with refractive index n necessary to support the metasurface [2], we apply the following substitutions to account for the first refraction [Fig. 3(a)]:

$$\sin U = \sin U^* / n, \quad \overline{AP} = n \overline{A^*P}, \quad L = L^* + \overline{AP}(n \cos U - \cos U^*) \quad (7)$$

By substituting Eqs. (7) and (6) into Eq. (5) we obtain the expression of the phase gradient for an aplanatic metasurface. For an object point at infinity we have $\overline{A^*P} \rightarrow \infty$, $\overline{A'P} \rightarrow f$, $\cos U = \cos U^* = 1$, and Eq. (5) becomes:

$$\frac{d\phi}{d\theta} = -n \frac{2\pi}{\lambda} \sin \theta \quad (8)$$

Equation (8) represents the phase gradient of a metasurface needed to focus a distant source of light without spherical aberration and coma.

An analysis of the aberrations of an aplanatic metasurface with $\text{NA} = 0.5$ is conducted to verify the correction introduced by the new design. The wavefront is calculated from the envelope of secondary spherical waves emitted from a distribution of scatterers placed at the surface of a spherical substrate [Fig. 3(a)] and excited by a parallel monochromatic light at $\lambda = 1.55 \mu\text{m}$ incident at an angle $\alpha = 10^\circ$ with respect to the optical axis. From the PSF and the MTF, shown in Figs. 3(b) and (c), we can see that the correction of coma improves the PSF and the resolution of the lens now reaches 30 cycles/mm (taking a contrast of 0.5).

5. Comparison between different designs

By tracing the rays through a conventional plano-convex lens, a flat lens, and an aplanatic metasurface with radius $\rho = 1 \text{ mm}$ and $\text{NA} = 0.5$ and under the same illumination condition used above ($\alpha = 10^\circ$), we ultimately compare the performance of the three different designs. For the conventional spherical lens [Fig. 4(a)] we assume a refractive index of $n = 3.5$ and a radius of curvature (R_c) as obtained from the Lensmaker equation ($R_c = 4.35 \text{ mm}$) [43]. For the flat lens [Fig. 4(b)] and the aplanatic metasurface [Fig. 4(c)] the substrate also has a refractive index $n = 3.5$ and the rays are refracted at the first interface; at the metasurfaces (green lines), the angles of refraction are calculated from the generalized laws of refraction [2,50], using the distribution of phase discontinuities given by Eq. (1) of [12] and Eq. (8), respectively. Progressive improvement is obtained for the three designs: the plano-convex lens is affected by both spherical aberrations and coma which produces an aberrated focal area for oblique illumination; the flat lens corrects spherical aberrations, but the coma is still present and gives rise to the typical comet-like asymmetrical focal spot; finally the aplanatic metasurface can compensate for coma as well, producing a good focus even for off-axis illumination.

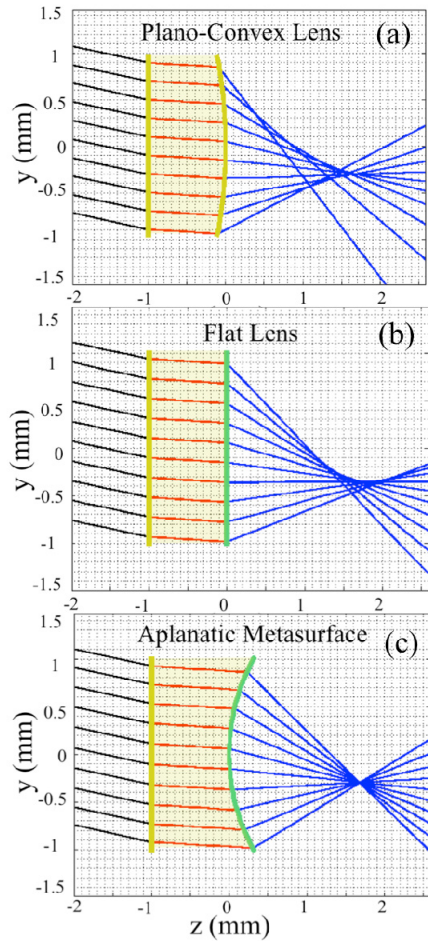


Fig. 4. Ray tracing plot for a plano-convex refractive lens (a), flat lens (b), and an aplanatic metasurface (c). The yellow-shaded areas represent the dielectric substrate ($n = 3.5$) and the green lines represent the metasurfaces. The parallel illumination forms an angle $\alpha = 10^\circ$ with respect to the optical axis, $NA = 0.5$.

In conventional bulk optics, an aplanatic lens is made of at least two or three air-spaced elements (doublet or triplet) [48]. An aplanatic metasurface offers the advantage of correcting spherical aberrations and coma in a single element. We have to emphasize that patterning nanostructures on a curved surface is a challenging step necessary for the realization of an aplanatic metasurface. Recently, thanks to the growing interests in different fields such as micro- and nano- optics, MEMS, biophotonics, etc., many manufacturing techniques have been adapted to non-flat substrates [51,52]. For example, a tiltable laser-lithography system has already been used to create a hybrid refractive and diffractive element on a spherical substrate [53]. This technique can reach a resolution suitable for the realization of metasurfaces in the infrared regime. Patterning of nano-resonators for visible light would require a resolution achievable with nano-imprint or electron beam lithography (EBL). A demonstration of EBL writing of ~ 100 nm features was made on a spherical shaped substrate thanks to a liquid phase deposition technique that guarantees coating of polymer resist with uniform thickness [54]. Finally, alternative fabrication strategies with higher throughput are based on pattern-transfer elements such as soft lithography [55–57] and flash imprint lithography [51].

6. Conclusion

In conclusion, we analyzed optical aberrations for focusing metasurfaces. We derived the *primary* (or *Seidel*) aberrations and calculated the point spread function (PSF) and modulation transfer function (MTF) and we showed that the flat lenses previously reported [12] are free from spherical aberrations creating perfect focusing for axial illumination. After analyzing the aberrations that arise from different illumination conditions and certain practical limitations, we proposed a design for an aplanatic metasurface patterned on a spherical interface to simultaneously correct spherical aberrations and coma.

To date, metasurfaces suffer from some limitations such as material losses, polarization dependence and reflection from the metasurface. Some of these limitations have already been overcome considering low-loss materials, multiple layers design [19] or by using elements that control simultaneously electric and magnetic polarization currents [7]. Due to the growing interest in ultrathin devices, we expect many developments towards more efficient flat lenses and other optical devices.

Acknowledgments

We thank Philipp Harms and Romain Blanchard for the helpful discussion.

This work was supported in part by Google, Inc. and by Charles Stark Draper Laboratory, Inc. under program SC001-0000000731.